Experimental and numerical characterization of an impure phase change material using a thermal lattice Boltzmann method

Alissar Yehya, Hassane Naji, Laurent Zalewski

Experimental and numerical characterization of an impure phase change material using a thermal lattice Boltzmann method

Alissar Yehya [a, b], Hassane Naji [c, d, 1], Laurent Zalewski [c, d]

[a] Harvard John A. Paulson School of Engineering and Applied Sciences, MA 02138, Cambridge, USA
[b] American University of Beirut (AUB), Department of Chemical and Petroleum Engineering, MSFEA, Lebanon
[c] Univ. Artois, Civil Engineering & Geo-Environment Laboratory (LGCgE- EA 4515), Technoparc Futura, F-62400 Béthune, France
[d] Northern Lille University France, LGCgE- EA 4515, FR-59000 Lille, France

Email addresses:

alissar_yehya@seas.harvard.edu; ay36 @aub.edu.lb

hassane.naji@univ-artois.fr

laurent.zalewski@univ-artois.fr

ORCIDs iD:

Alissar Yehya https://orcid.org/0000-0001-9956-3636

Hassane Naji http://orcid.org/0000-0002-5994-7958

Laurent Zalewski https://orcid.org/0000-0002-7298-3224

[1] Corresponding author at Univ. Artois, Laboratoire Génie Civil & géo-Environnement (LGCgE - EA 4515) Technoparc Futura, F-62400 Béthune, France.
E-mail address: hassane.naji@univ-artois.fr (H. Naji).
Tel.: + 33 611 267 983

Towards experimental and numerical characterization of an impure phase change material using a thermal lattice Boltzmann method Abstract

Of the phase change materials (PCMs) that regulate ambient temperature while reducing energy consumption, Octadecane is a good candidate because of its transparency properties and its adequate melting temperature. This study aims to characterize, through an approach combining numerical simulation and experiment, the behavior and thermo-physical properties of n-Octadecane. The approach takes into consideration the natural convection and the use of PCM's experimentally-obtained enthalpy-temperature curve that includes the supercooling and soluble impurities effects. The model uses the thermal lattice Boltzmann method based both on a partial bounce-back and an enthalpy formulation while including the experimental relationships. The numerical and experimental results exhibit good agreement. The approach adopted allows to highlight the behavior of the PCM to better characterize its thermo-physical properties.

Keywords: Phase change materials (PCMs), Lattice Boltzmann method (LBM), Convection, Supercooling, Impurities.

Nomenclature

c	specific heat capacity (J/kg.K)
c_s	lattice sound speed (lu/ts)
e_i	streaming particle velocity in i-direction (lu/ts)
f_i	particle distribution function of fluid (-)
g_i	particle distribution function of temperature (-)
g	gravity's acceleration (m/s^2)
h	specific enthalpy (J/Kg)
k	thermal conductivity (W/m.K)
L	latent heat of fusion (J/kg)
lu	lattice unit of length
m	total masse (kg)
PCM	phase change material
PDF	particle distribution function
T	temperature (K)
T_a	melting temperature of pure PCM (K)
T_0	initial temperature (K)
T_m	melting temperature of impure PCM(K)
T_P	imposed temperature on two faces of the sample (K)
t	time (s)
ts	lattice unit of time
U	macroscopic velocity (m/s)
u, v	x-, y-velocity component (m/s)
x	cartesian (m)
X_i	impurities' fraction
Greek symbols	
α	thermal diffusivity (m^2/s)
β	thermal expansion coefficient (K^{-1})
Δt	time step (s)
Δx	space step (m)
ε	liquid fraction (-)
ν	kinematic viscosity (m^2/s)
ρ	macroscopic density (kg/m^3)
ω_i	weight coefficient (-)
τ_f, τ_h	dimensionless lattice relaxation times
Superscripts/subscripts	
eq	local equilibria
l	liquid phase of PCM
m	melting
s	solid phase of PCM
w	wall

36

1. Introduction

The global population growth has led to a high energy demand and increased CO_2 emissions triggering a major environmental crisis. The energy use in buildings accounts for a large share of the total end use of energy, with an average consumption of about 50% of all raw materials owned in the world [1]. This percentage would differ depending on the region, and is equal to 40% in Europe, 30% in USA, and reaches 70% in undeveloped countries [2]. Energy consumption for thermal comfort in buildings rises with increasing in user demand for comfort conditions. This rise in, both, energy consumption and CO_2 emissions thus promoted a new policy aimed at creating more sustainable buildings [3]. Scientists all over the world are in search of new and renewable energy sources. One of the options is to develop energy storage devices, which are as important as developing new sources of energy. Thermal energy storage does not only reduce the temporal gap between supply and demand, but it also improves the performance of energy systems and plays a significant role in conserving energy [4]. Such storage can be achieved either by using sensible heat or thermo-chemical heat or latent heat. Among these different methods, the latent thermal energy storage (LTES) method, using phase change materials (PCMs), is the most preferred and the most widely used at present [5, 6] mainly for their application for heating and cooling of buildings [4, 7-11]. PCMs can be used for temperature regulation and their high storage capacity can reduce energy consumption in buildings, and thereby contribute to the reduction of CO_2 emissions.

Recently, interest in the use of Octadecane in latent heat systems and building materials has increased. Its choice is mainly due to its transparency properties and its melting temperature, which lies within the thermal comfort of human beings. The original idea is to fill Plexiglas enclosures with PCM having transparency properties, and thereby create a wall of a building façade or windows that benefits from solar gains. For PCMs in windows, paraffin-based organic materials are the most interesting since they are transparent in the liquid state and translucent in the solid state. For that, it is interesting to investigate more on Octadecane as a PCM. The main task

throughout this research is to develop a numerical model that matches the experimental results and helps infer some thermo-physical properties that are difficult to predict via single experiments, example: the thermal contact resistance, conductivity in liquid phase, the degree of supercooling, heat transfer coefficient, etc. Following this, the model can be also used to enhance and optimize PCM performance in practical applications. Note that, at this stage, the heat transfer by radiation is not considered since our experimental apparatus induces heat through attached plates controlled by thermo-regulated baths (see Section 4). Actually, the study of such materials will involve the characterization part, as our present study, and an application part where the experimental setup will be different and will follow appropriate climatic and external conditions and adequate geometric scales. Both tests and studies are required for this material to reach a mature state for practical applications.

Thus, prior to the large-scale practical application of this technology, it is crucial to consider certain issues in the stage of research and development [4]. The experimental investigation of some PCMs showed the presence of some phenomena that could affect the performance if not considered in the design, namely supercooling, convection and impurities. When supercooling occurs, the start of solidification is delayed, and the liquid solidifies at a temperature below its freezing temperature. This can lead to a mismatch between the design and the real behavior of the PCM [12]. Most of the theoretical heat transfer modeling of PCM energy storage systems is based on the conjecture that the supercooling degree is negligible or even completely absent. However, recently published researches [12-14] indicate that even a relatively small degree of supercooling might result in a significant undesirable effect on the heat release rate as a function of time, reducing the thermal efficiency of the system. Therefore, it is important to provide reliable theoretical modeling of supercooling in PCM for a more adequate design.

Another important phenomenon, ignored in some numerical models, is the natural convection in the liquid phase. If PCMs with high Prandtl number are used, e.g. Octadecane, it is very likely to have convection even in small samples. This is because the relative thickness of the momentum

boundary layer is much more than the thermal one. Hence, convection will be dominant with momentum diffusing more quickly compared to heat. In addition, soluble impurities, if they exist, may lead to depression in melting point thus altering the temperature-enthalpy curve, so that the traditional piecewise function can no longer be used. Also, the thermal contact between different materials in the system can have similar effects on the enthalpy curve. Therefore, using a simplified model may fail to successfully predict the phase change process, if the aforementioned phenomena are present. Thereby, the main aim targeted here is to provide an improved model that accounts for supercooling, convection and the modified enthalpy-temperature curve. To carry out this work, we consider the thermal lattice Boltzmann method (TLBM) [15-20] based on a partial bounce-back (PBB) approach [21-23] supplemented with an enthalpy-based model. This enhanced model provides a more accurate simulation of phase-change materials, can better predict the solidification and melting processes, and thus match the experimental results.

The paper is organized as follows: Section 2 provides a literature review on challenges in modeling phase-change materials. Section 3 is devoted to the lattice Boltzmann method adopted herein to achieve the numerical solution while supplementing the appropriate enhancements. The experimental setup with equipment and the measurement method is outlined in Section 4. Section 5 presents the experimental determination of the thermo-physical properties of Octadecane: conductivities, specific capacities, latent heat of fusion, and the analysis of the heat flux curves. Thorough discussions of the confrontation between numerical and experimental results are presented in Section 6. Finally, Section 7 concludes the paper by providing key findings based on the dual experimental and numerical approach.

2. Challenges of modeling of phase-change materials

PCMs have various possible applications ranging from temperature stabilization to energy storage. Though many pure chemical elements can be used as PCMs, the majority often consists of a mixture, or contains at least soluble impurities. The main reason for creating a PCM as a mixture of various substances is to achieve a desirable melting temperature for a particular application.

However, these mixed or impure PCMs require accurate and reliable methods for determining their thermo-physical properties, which represents a significant issue that considerably affects the accuracy and credibility of the corresponding studies. Numerical modeling can help in determining some of these properties. However, other serious complexities interfere in the modeling of phase change materials, which makes it a real challenge.

Many macroscopic mathematical modeling schemes for solidification/melting problems can be found in the literature [23-25]. Early efforts initiated with the moving/deforming grid approach [24, 25] in which independent conservation equations for each phase are initially formulated and are subsequently coupled with appropriate boundary conditions at the interfaces. However, such multiple region solutions require the existence of discrete interfaces between the respective phases. In fact, a major difficulty in their implementation [26] is associated with tracking the phase interfaces (which are generally unknown functions of space and time). Additionally, a serious limitation exists for modeling phase change behavior of multi-component systems, since they do not exhibit a sharp interface between solid and liquid phases. Moreover, solidification occurs over extended temperature ranges and solid formation often occurs as a permeable crystalline-like matrix, which coexists with the liquid phase. Otherwise, there are the fixed-grid models, using finite element (FE) or finite volume (FV) methods [24, 27]. A separate equation for the liquid fraction evolution is solved, which implicitly specifies and updates the interfacial locations with respect to space and time. The fixed grid method is relatively simple, versatile, practical, adaptable and easily programmable [11]. It can easily handle melting or solidifying materials over a range of temperatures. The latent heat evolution is accounted for in the governing equation by using, either enthalpy method [12, 23], heat capacity method [13, 28], temperature transforming model [14], heat source method [24, 25], or other methods.

On the other hand, the multi-scale mesoscopic lattice Boltzmann method (LBM) has emerged to offer huge potential for solving complex thermo-fluidic problems involving morphological

development of complicated phase boundaries [21-23, 29-33] and recovers the Navier-Stokes and energy equations. In addition, it has been witnessed that the LBM stands out in major fields of classical fluid dynamics: multiple-scale flows and heat transfers with or without phase change process. Its advantage, compared to a classical based-continuum formulation, is that it operates at a mesoscopic level, which incorporates micro and meso-scale physics of phase transitions, and bypasses the explicit calculation of the pressure equation, leading to time-efficient computational simulations. Further, LBMs are inherently transient and parallelizable, which renders their suitability to address phase change processes over large-scale computational domains [34]. Moreover, by adopting partial bounce-back approach with enthalpy formulation [15], LBM treats phase-change as flow in porous medium. Extensive work has been done to simulate fluid and heat flow in porous media using LBM [35, 36]. The liquid fraction calculated through an enthalpy formulation designates the porosity in the mushy zone and helps tracking fusion front and simulating convection. The local nature of the method allows adding local complexities where necessary.

3. Numerical Model

3.1. Enthalpy-temperature relationship

The most common enthalpy/temperature relationship is often translated as a piecewise function in the case of pure materials. However, even a small amount of impurities can lead to a significant change in the enthalpy curve shape, with a depression of the melting temperature followed up by a melting range. Hence, melting point analysis can provide information on the sample purity [37]. In other words, a substance including soluble impurities will be prone to “melting point depression”. This is related to the intermolecular forces within the material. As the solid impurity increases, its structure will be more disrupted, and hence will result in a greater variation in intermolecular forces throughout different areas of the solid. The effect will be that the melting temperature is lower than

that of a pure material, and the solid melts over a wider range of temperatures. Note that this is not the case for insoluble impurities. The latter will have no effect on the compound's melting point.

When soluble impurities exist, the model can be dealt as a binary mixture, with one component having very small portion compared to the other. Thereby, we can calculate the depression in the melting temperature (ΔT_{am}) as follows [37]:

$$\Delta T_{am} = T_a - T_m = R T_a^2 X_i / L_f \tag{1}$$

where T_a is the melting point of a 100% pure material, T_m is the lowered melting point of the impure material, L_f (*J/mol*) is the molar heat of fusion, R (= 8.314 *J/mol/K*) is the ideal gases universal constant, and X_i is impurities' fraction in the considered material. In this work, this can be used as a pre-estimate of the real melting temperature of the studied sample with respect to the expected melting temperature in literature.

It seems obvious that impurities' percentage in a material alters the enthalpy curve of a substance and consequently affects the resulting heat flux. The peak of the heat flux curves becomes wider and shorter as the impurity increases while maintaining the same underlying area (under it), which is related to the melting enthalpy.

- **Enthalpy-temperature relationship for pure PCMs**

The variation of enthalpy vs. temperature of a pure material is:

$$\frac{dh_{pcm}}{dT} = \begin{cases} c_{s,pcm} & for \quad T < T_a \\ c_{l,pcm} & for \quad T > T_a \end{cases} \tag{2}$$

It should be noted that dh_{pcm}/dT tends to infinity when T approaches T_a.

- **Enthalpy-temperature relationship for non-pure PCMs, i.e. with soluble impurities**

For an impure material, the variation of the enthalpy vs. temperature can be written as [38-40]:

$$\frac{dh_{pcm}}{dT} = \begin{cases} c_{s,pcm} - (c_{s,pcm} - c_{l,pcm}) \dfrac{T_m - T_a}{T - T_a} - L_f \dfrac{T_m - T_a}{(T - T_a)^2} & for \quad T \le T_m \\ c_{l,pcm} & for \quad T > T_m \end{cases} \tag{3}$$

The resulting expression of the enthalpy becomes:

$$h_{pcm}=\begin{cases} c_{s,pcm}(T-T_m)+(c_{l,pcm}-c_{s,pcm})(T_a-T_m)\ln\left[\dfrac{T-T_a}{T_m-T_a}\right]+L_f\left[\dfrac{T_m-T_a}{T-T_a}\right]+H_0 & for \quad T\le T_m \\ c_{l,pcm}(T-T_m)+L_f+H_0 & for \quad T>T_m \end{cases} \tag{4}$$

where T_a and T_m are the melting temperatures of pure and impure PCMs, respectively. However, L_f is the latent heat of fusion, H_0 is the enthalpy at T_E, which denotes the onset of melting.

3.2 Thermal lattice Boltzmann model (TLBM)

The Lattice Boltzmann method (LBM) is a mesoscale discrete model that has become an increasingly popular tool for simulating fluid flows with and without heat transfers [15-20]. It consists of simulating the statistical behavior of a set of particles on a lattice with finite velocities. This evolution is carried out in a cycle of "streaming" (advection) and "collision" steps. The essential interpretation of such an approach is that it is a special finite difference form of the continuous Boltzmann equation. Furthermore, it allows providing macroscopic fluid properties, such as density, velocity, pressure, etc., through weighted averages, or moments, of the particle distribution for all discrete lattice velocities. The single relaxation time (SRT) lattice Boltzmann model (also called the lattice Bhatnagar-Gross-Krook (LBGK) model) [41, 42] for incompressible thermal flows leans on two distribution functions (DFs) with their corresponding evolution equations to solve the evolution of the two mesoscopic particle distribution functions, f_i and g_i, via the discretized lattice Boltzmann equation as following:

$$f_i\left(x+e_i,t+1\right)=f_i\left(x,t\right)-\tau_f^{-1}\left(f_i\left(x,t\right)-f_i^{eq}\left(x,t\right)\right)-\tau_f\beta g\left(T-T_0\right)/\rho\Delta T \tag{5}$$

$$g_i\left(x+e_i,t+1\right)=g_i\left(x,t\right)-\tau_h^{-1}\left(g_i\left(x,t\right)-g_i^{eq}\left(x,t\right)\right)+S_h^g \tag{6}$$

where e_i is the microscopic particle velocity in the i-direction, τ_f and τ_h are the dimensionless relaxation times, and f_i^{eq} and g_i^{eq} are local equilibrium distributions functions that can be computed from:

$$f_i^{eq} = \rho\omega_i\left[1+\frac{3(\vec{e}_i.\vec{U})}{c_s^2}+\frac{9(\vec{e}_i.\vec{U})^2}{2c_s^4}-\frac{3(\vec{U}.\vec{U})}{2c_s^2}\right] \quad (7)$$

and $g_i^{eq} = T\omega_i\left[1+\frac{\vec{e}_i.\vec{U}}{c_s^2}\right]$ (8)

where $\omega_i = \begin{cases} 4/9 & for \quad i=0 \\ 1/9 & for \quad i=2,4,6,8 \\ 1/36 & for \quad i=1,3,5,9 \end{cases}$ and $e_i = \begin{cases} (0,0) & for \quad i=0 \\ (0,\pm1) & for \quad i=2,4 \\ (\pm1,0) & for \quad i=1,3 \\ (\pm1,\pm1) & for \quad i=5,6,7,8 \end{cases}$ (9)

are, respectively, the weight coefficient and the velocity vector of the D_2Q_9 model; $\vec{U}(u,v)$ is the macroscopic velocity, with, u and v representing velocities in the x- and y -directions, respectively. Note that the relaxation times τ_f and τ_h can be determined via $\nu_{lattice} = c_s^2\Delta t(\tau_f - 0.5)$ and $\alpha_{lattice} = c_s^2\Delta t(\tau_h - 0.5)$, c_s being the lattice sound speed. It should be noted that, the lattice viscosity and thermal diffusivity are selected so as to conform to the intended Prandtl number Pr $\left(=\nu_{lattice}/\alpha_{lattice}\right)$. Likewise, the additional force term related to Boussinesq force F_b is incorporated in the model by shifting the velocity field by a term of $F_b\tau_f/\rho$ as proposed by Shan and Chen [43], where F_b $\left(=-\beta g(T-T_0)/\Delta T\right)$. By this treatment, there is no need to add a force term to the collision operator. On the other hand, in g-distribution function, the source term is treated as per the method proposed by Luo [44]. Hence, the resulting force in the LBM frame will be: $S_h^g = -\omega_t S_h$ with S_h $\left(=Ste^{-1}\partial\varepsilon/\partial t\right)$ being the source (or sink) term that handles the phase-change. Note that, we performed tests on the temperature and liquid fraction to insure that they converge within an acceptable tolerance after one iteration for the parameters set considered in this study.

It is worth recalling that the description and validation of the model adopted herein can be found in [21, 45, 46]. The numerical model will calculate the temperature and velocity fields for both

conduction and convection heat transfer modes. Afterwards, the liquid fraction will be calculated from the enthalpy while taking into consideration the impurities' presence. Hence, the enthalpy h is calculated from equation (4).

The liquid fraction (ε) is computed as:

$$\varepsilon = \begin{cases} 1 & if\ \varepsilon_1 = 1 \\ \varepsilon_2(h) & if\ \varepsilon_1 = 0 \end{cases} \tag{10}$$

where ε_1 is an indicator parameter that is equal to 1 as long as nucleation did not occur for the solidification phase. For nucleation to occur the temperature should fall below the nucleation temperature T_{nuc}, where the degree of supercooling is the estimated as ($T_m - T_{nuc}$). Note that this happens only in solidification, so that the solidification and melting curves are defined according to different indicators. The above numeric indicator controls what enthalpy curve is used for the calculation of liquid fraction according to Fig. 3, and then,

$$\varepsilon_2(h) = \begin{cases} 0 & for\ h < h_s = c_{s,pcm} T_E = H_0 \\ \dfrac{h - h_s}{h_l - h_s} & for\ h_s \le h \le h_l = h_s + L_f \\ 1 & for\ h > h_l \end{cases} \tag{11}$$

It is useful to recall that, in the current model, the solid and liquid phases are defined according to the liquid fraction value. Therefore, a mushy zone state is assigned when the value of ε is between zero and one. In this case, the velocity field is partially bounced back and the macroscopic velocity is modified [15, 45, 46]. The procedure for implementing the partial bounce-back approach is described in [45, 46].

For the velocity field, the non-slip BCs are used for all the cavity walls. These are performed by the on-grid bounce-back (BB) boundary conditions:

$$f_i(x_w, t+1) = f_j(x_w, t) \tag{12}$$

x_w being the fluid node adjacent to the wall, and i and $\bar{j}$ represent two opposite lattice directions on the boundary site. Note that the BB conditions apply to the DF in non-parallel directions at a solid wall.

To specify a constant temperature at the left and right walls, we use the method proposed by Inamuro *et al.* [47]. Its principle is to substitute unknown DFs for a boundary point with local equilibrium values using an adjusted temperature to set the defined temperature at that point. Specifically, the adjusted temperature on the left side can be expressed as:

$$T' = \frac{6}{1-3v_{w,x}}(T_h - \sum g_k) \tag{13}$$

$v_{w,x}$ being the computed near-wall velocity, and $g_{\bar{p}}$ represents a known distribution function. Hence, the unknown DFs $g_{\bar{p}}$ are computed by $g_{\bar{p}} = T'\omega_i(1+\vec{e}_i.\vec{U}/c_s^2)$. As for the adiabatic BCs, the Neumann BCs are achieved using the BB boundary conditions for the distribution g_i, as prescribed for f_i.

In the nearly incompressible formulation, the basic thermo-hydrodynamic properties, such as density ρ, momentum density, ρU, and temperature, T, are defined as moments of the DFs, f_i and g_i, as follows,

$$\rho = \sum_{i=0}^{i=8} f_i, \qquad \rho U = \sum_{i=0}^{i=8} e_i f_i, \qquad T = \sum_{i=0}^{i=8} g_i \tag{14}$$

To simulate the presence of a mushy zone (co-existence of liquid and solid), a step is added to mimic the bounce-back at a lattice node [23, 45, 46]. This condition redirects the incoming fluid packets prior to the collision step, as follows:

$$f_i^{out}(x,t) = (1-\varepsilon) f_i^{col} + \varepsilon f_i^{in}(x,t)$$

where f_i^{in} and f_i^{out} denote the incoming and outgoing fluid packet densities at a node.

This ensures that for a completely liquid phase ($\varepsilon = 1$), a normal collision is conducted. However, when it is completely solid ($\varepsilon = 0$), the flow is bounce-backed and blocked, whereas for values between 0 and 1, the flux is partially bounce-backed according to the solid fraction estimated at the node. Such a scheme has been verified in our previous work compared to analytical solutions and other numerical methods [21-23, 40, 41].

The velocity field is then modified in the mushy zone and expressed in terms of the in-coming fluid packet densities,

$$U^* = \varepsilon . U \tag{15}$$

This modified velocity is in accordance with the requirements of the partial bounce-back approach [23, 45, 46]. As a result, the flow in the mushy zone will be dealt as flow in a porous medium and will therefore be governed by Darcy's law as proved by derived analytical solutions [23, 45, 46].

4. Experimental Setup

Recall that the main task targeted here is to develop a mutually compatible experimental and numerical method to characterize the studied PCM. The major enhancement in the current numerical model is to add natural convection and supercooling, adopt variable thermo-physical properties, and use the real enthalpy curves corresponding to the considered PCM (viz. Octadecane). Let's point out that this PCM is an alkane hydrocarbon of chemical formula is $CH_3(CH_2)_{16}CH_3$ with Prandtl number is about 50. In general, for high Prandtl values, the momentum diffusivity dominates, and convection seems very efficient in transferring heat (energy).

To solve this physical problem, the TLBM, for phase change in multi-layered materials, is used herein. However, before confronting numerical simulations findings, we perform experiments on

the Octadecane to characterize its main thermo-physical properties: conductivity (solid and liquid), heat capacity (solid and liquid), and latent heat of fusion. The numerical model, hereby, helps us to determine both the real enthalpy curve and the degree of supercooling in the material. Figure 2 shows the schema of the experimentally studied sample of Plexiglas containing Octadecane as PCM. Tables 1 and 2 gather the properties of Octadecane and Plexiglas, used in the numerical model, as per the literature [48, 49] and verified experimentally with an acceptable tolerance.

The experimental setup and its associated equipment, used in this work, are schematically depicted in Figs. 2 and 3(a, b). The studied phase-change material, viz. Octadecane (99% pure), is placed inside a parallelepiped Plexiglas enclosure and prone to a temperature gradient through exchange plates controlled by two thermo-regulated baths (Julabo Model 34 HE - 1kW with a precision of about ±0.01 °C)) that define thermal conditions (see specifications in [50]). The exchange aluminum plates (500 *mm* × 500 *mm* × 19 *mm*) allow imposing temperature variations, with respect to selected time scales, on the two dominant faces (left and right faces). The upper and bottom faces, of the studied sample, are insulated by a 14.5 cm-thick polystyrene (a thermally insulating material). Such insulation also serves to minimize the heat transfer from the sample lateral faces into the surrounding medium. This is the guarded hot plate approach principle, often used when characterizing the thermal performance of PCM samples. The flux-meters used herein are "tangential gradients flux meters". The inserted sensors (Captecv, France) on the sample's both sides were pre-calibrated (using the comparative method) with a precision of about 2%, using the device described by [51]. Their surface, thickness and sensitivity are 210×140 mm^2, 0.2 *mm* and 124 $\mu V.W^{-1}.m^{-2}$, respectively. The various sensors are connected to a multichannel multimeter (Keithley 2700) adapted to low level signal measurements. Experimental data are scanned at regular and adjustable time steps of 10 s. The adopted experimental setup permits the simultaneous measurement of heat fluxes and temperatures through the different faces. Note that data acquisition is facilitated by a PC running LabVIEW for further analysis.

According to the thermal program applied to the sample, it is possible to characterize the apparent thermal conductivity, the specific heat capacity, the phase change temperature and latent heat of the sample. Indeed, the experimental set-up permits to impose temperature loading on each face of the studied sample. Simultaneous measurements of temperatures and heat fluxes exchanged during heating and cooling processes allow the determination of the apparent thermo-physical properties. The characterization also yields to the determination of conductivities and heat capacities when the PCM is in solid or liquid state. During the phase change, temperature and the latent heat can be determined via proven methods [50 - 52], to name few.

5. Obtaining Octadecane thermo-physical properties

5.1. Thermal conductivity and thermal contact resistance in solid phase

For the solid phase test, we impose, using the previous experimental setup, temperatures of T_G = 10 °C and T_D = 15 °C (below melting temperature) on the left and right faces, respectively, until a thermal steady state is reached. The heat fluxes are initially constant. At a particular time, an increase of 5°C in temperature is imposed in both thermo-regulated baths linked to the plate heat exchangers. This will induce an increase of temperature in the material, before reaching again a thermal equilibrium. The sample would thus store energy (sensible heat) between these two permanent steady states. A similar experiment is performed to determine the thermal conductivity in the liquid phase. The sample is also subjected to a temperature increase of 5°C starting from T_G = 30 °C and T_D = 35 °C, insuring temperatures higher than the melting temperature of the Octadecane. The subjected thermal loading ramp and the resulting heat fluxes are shown in Fig. 4(a, b).

The thermal conductivity λ can be determined depending on the sum of heat fluxes and the temperature difference, using the following relation [53],

$$\lambda = \sum \varphi L / 2\Delta T \tag{16}$$

where φ is the heat flux density in W/m^2 and L is the thickness of the sample.

It is useful to mention that the used method involved simultaneous measurements of the heat fluxes and temperatures on both sides of the differentially heated sample. Compared to conventional methods of determining the thermal conductivity in steady state, this method is four times faster [53]. The exact term for the quantity measured is "thermal transmission", which, depending on the material being measured, can have components of convective, radiative and conductive heat transfer; it is commonly referred to as the effective or apparent thermal conductivity.

The heat sensor is made of a thin material with a high thermal conductivity (copper). Thermal contact resistance (or contact resistivity) may cause huge errors of thermal conductivity measurements if it is not taken into account. Moreover, when there are two different material layers, a thermal resistance exists on their interface. It is more obvious in the case of two solids. In case of thermal insulation materials (small conductivity) the sample's thermal resistance is large and thermal contact resistance can be neglected. But, in case of higher conductivity materials *(> 0.1 W/mK)*, the thermal contact resistance becomes significant compared to the sample's thermal resistance and cannot be neglected [54]. Hence, it is important to estimate this effect for accurate results.

The resistance of the sample can be defined by:

$$R_{eq} = 2R_c + 2R_{pl} + R_{oct} \tag{17}$$

where R_c, R_{pl}, and R_{oct}, are respectively the thermal resistivity contact, resistance of Plexiglas and Octadecane. We first neglect the thermal contact resistivity. Then,

$$R_{eq} = \frac{L}{\lambda_{eq}} = \frac{2L_{pl}}{\lambda_{pl}} + \frac{L_{oct}}{\lambda_{oct}} \tag{18}$$

Here, we apply Eq. 18 to calculate the equivalent conductivity of the sample (Plexiglas + Octadecane). The literature properties of Plexiglas are gathered in Table 1, and those for

Octadecane are in Table 2. The resultant conductivity in the solid case is: $\lambda_{eq} = 0.167\ W/(m.K)$. Hence, by applying Eq. 18, we get $\lambda_{oct} = 0.152\ W/(m.K)$. This value is very far from the conductivity of Octadecane reported in the literature [48, 49]. The error is probably due to ignoring the thermal contact resistivity. As stated before, when testing samples of moderate thermal conductivity (λ~ 0.1-10 W/(m.K)) the thermal contact (or interface) resistance must be addressed, otherwise significant errors will result. Since we are not sure about R_c, we will suppose range of values of $1/R_c = 50 - 100$. Thus, as we change R_c , we obtain different thermal conductivities of solid Octadecane: ($R_c = 1/100$; $\lambda_{oct} = 0.219\ W/(m.K)$; ($R_c = 1/70$; $\lambda_{oct} = 0.27\ W/(m.K)$; ($R_c = 1/60$; $\lambda_{oct} = 0.31\ W/(m.K)$; ($R_c = 1/50$; $\lambda_{oct} = 0.39\ W/(m.K)$.

From here, we can realize the major impact of considering the thermal contact in calculating the conductivity of Octadecane, which has a relatively moderate conductivity. The estimated values of λ_{oct} are plotted versus R_c in Fig 5a. The value in the literature for the conductivity of Octadecane is $\lambda_{oct}\ (solid) = 0.356\ W/(m.K)$ which corresponds mostly to around $R_c = 1/60$. It is worth mentioning that the contact resistances here occur between the flux sensors and Plexiglas, and also between Plexiglas and solid PCM. This is applicable for the 4 faces of the enclosure. However, since we take a 2D model, we ignore the effect of resistance on the upper and lower faces.

5.2. Thermal conductivity, thermal contact resistance and convection in liquid phase

As in the previous procedure, we calculate the conductivity in liquid Octadecane. The Flux density and surface temperatures are plotted in Fig 4b. The estimated value by Eq. 18 is λ_{app} (liquid) $= 0.22\ W/(m.K)$, which can be seen as an apparent conductivity. It is important to recall here that the quantity measured may have a convection component. Therefore, we seek to, theoretically, prove the existence of convection in the liquid state. This would check the high value of the apparent conductivity in liquid phase, and then to confirm this experimentally and numerically.

- **Theoretical evaluation of the convection**

We need to calculate $Ra_H = \beta g \Delta T H^3/\alpha\upsilon$ for the above problem ($A=H/L \approx 20$), corresponding to the considered sample. This gives us an idea about the mechanism of heat transfer, within the sample, and on the effect of the fluid flow, following the scaling laws [55]. In such a tall enclosure the convection is usually ignored. Here, our aim is to check the importance of considering convection theoretically, numerically, and experimentally.

According to the scaling laws [55], the parameter Ra_H needs to be calculated and to H/L:

$(Ra_H)^{1/4} = (\beta g \Delta T H^3/\nu\alpha)^{1/4} = (1.415\times10^{10})^{1/4} \approx 345.$

$(Ra_H)^{-1/4} = (\beta g \Delta T H^3/\nu\alpha)^{-1/4} = (1.415\times10^{10})^{-1/4} \approx 0.003$

$H/L = 20.2$, so $(Ra_H)^{-1/4} < H/L < (Ra_H)^{1/4}$.

So, the flow pattern is expected to show a boundary layer on all four walls, with one core remaining stagnant. The dominant heat transfer mechanism is "boundary layer convection" with a significant effect of the fluid flow. To calculate the Nusselt number, we can use an adequate empirical formula. Since $Ra_L = \beta g \Delta T H^3/\nu\alpha = 3.43\times10^5$, with $10< H/L < 40$, $1 <Pr < 2\times10^4$, $10^4 <Ra_L <10^7$, then:

$$\overline{Nu}_L = 0.42\, x Ra_L^{1/4}\, x\, Pr^{0.012}\, x\left(H/L\right)^{-0.3} \qquad (19)$$

This relationship allows to deduce $\overline{Nu}_L = 4.33$ with $Ra_L = \beta g \Delta T L^3/\nu\alpha$. This reveals that the convective heat transfer is four times stronger than the conductive one. Once again, this shows that the convection is the dominant mechanism in this problem. The apparent conductivity measured by Eq. 18 has a convection contribution, and we can state that it is not the equivalent conductivity of the sample.

- **Experimental investigation of the convection**

To achieve this, we perform a new experiment. We inject in the Plexiglas enclosure of Octadecane, described in Fig. 2, silver coated hollow glass spheres, and allow them to settle down. Using Particle Image Velocimetry (PIV) system, we trace the flow of the particles inside the enclosure. In the case of liquid Octadecane, due to the presence of convection, and as expected, the

412 powder circulates inside liquid Octadecane. In contrary, if conduction was the dominant mode, the
413 powder would have stayed at the bottom, and no motion would have been noticed.
414 After proving the presence of convection, we will estimate the value of the conductivity of liquid
415 Octadecane, by the aid of the numerical simulations.
416 ▪ **Numerical assessment of the convection**
417 The implemented LBM numerical model is used to evaluate the convection in liquid Octadecane
418 within the Plexiglas enclosure. Thus, the average Nusselt number ($\overline{Nu}_L$) value on the Octadecane
419 interface is 4.81. Such a value seems close to that estimated empirically by the order of 10%.
420 The average equivalent conductivity for natural convection can be estimated via the following
421 relationship [55]:

422 $$\frac{\lambda_{app}}{\lambda_{eq}} \approx \frac{Q_{LBM,conv}}{Q_{LBM,cond}} \quad (20)$$

423 where λ_{app} and λ_{eq} are the apparent and equivalent conductivities of liquid Octadecane. Note that,
424 by apparent here, we mean that it contains the convection contribution. As for the equivalent, we
425 point to the conductivity calculated for the sample (Plexiglas + Octadecane). To compute the ratio,
426 we implement two models. The first is for convection (with a Boussinesq force evaluated by the
427 corresponding *Ra* value), and the second is a pure conduction model (without the Boussinesq force,
428 insuring a zero-velocity field). The simulation results do not depend on the selected value of
429 conductivity, since in LBM we assign a fixed Prandtl number of 50. The main aim here is to
430 evaluate the effect of including the Boussinesq force that designates the convection. This method
431 is only an approximation. The calculated ratio is $\lambda_{app}/\lambda_{eq} = 1.76$, hence the value of the equivalent
432 conductivity is $\lambda_{eq} = 0.125$ *W/mK*. Here, the thermal contact resistance occurs only between the
433 flux sensors and the Plexiglas. Now we use Eq. 18 with different trials on the thermal contact
434 resistance to get: $R_c = 1/100$; $\lambda_{oct} = 0.123$ *W/(m.K)*; $R_c = 1/70$, $\lambda_{oct} = 0.137$ *W/(m.K)*;$R_c = 1/60$;
435 $\lambda_{oct} = 0.151$ *W/(m.K)*; $R_c = 1/50$; $\lambda_{oct} = 0.162$ *W/(m.K)*.

The conductivity of liquid Octadecane is $\lambda_{oct} = 0.148\ W/(m.K)$ in literature. So in both liquid and solid cases the closest calculated value of conductivity is obtained when considering $R_c = 1/60$. Fig. 5b shows the estimated values of λ_{oct} for the liquid Octadecane versus the thermal contact resistance. As deduced, the effect of thermal resistivity contact is much more in the case of the solid state, where there is a solid-solid contact. Thereby an interface of the air gap may rise in between. From our approach, the conductivity of solid and liquid Octadecane are $\lambda_{oct}\ (solid) = 0.31\ W/(m.K)$ and $\lambda_{oct}\ (liquid) = 0.151\ W/(m.K)$, respectively with $R_c = 1/60$. However, we should still consider border effects for more accuracy.

5.3. Specific heat capacity

The temperatures and the heat fluxes evolution on both sides of the sample, when Octadecane is in the solid and the liquid phases are represented in Fig. 4. A symmetrical behavior of heat fluxes and temperatures measured on both faces of the sample can be observed, which correspond to the results classically obtained with a solid material without phase change.

Initially, the sample is isothermal (at a thermal equilibrium state), and then a temperature change is imposed on its both sides. This induces a thermal evolution of the system in an asymptotic way towards a second thermal steady state. Also, it should be noted that the heat fluxes evolve quickly when the temperatures of the sample are increased and then converge to a second thermal equilibrium state obtained at the end of the test. The specific heat capacities of the sample are obtained starting from the determination of the sensible heat accumulated by the material between the imposed temperatures. The sensible heat is calculated by integrating the difference in heat fluxes between the initial and the final state using the following relationship:

$$Q = \frac{1}{\rho L}\int_{T_{init}}^{T_{end}} \Delta\varphi = \sum_i C_{p,i}\left(T_{end} - T_{init}\right) \tag{21}$$

where $\Delta\varphi$ represents the cumulative heat rate entering the sample and C_p is the apparent specific heat capacity ($kJ/(kg.°C)$).

The calculated specific heat capacity of Octadecane in solid and liquid phases are: $c_{oct,solid} = 1925$ $kJ/(kg.°C)$ and $c_{oct,liquid} = 2365$ $kJ/(kg.°C)$. It is noted that these values are consistent with those available in the literature.

5.4. Analysis of the heat flux with phase-change

To analyze the heat flux in the presence of a phase change, we use a four-hour ramp. The sample is initially at 15.8 $°C$, then the both plates' temperature T_p is increased from 15.8 $°C$ to 40 $°C$ in 4 hours $(4h)$. Then a constant loading of 40 $°C$ is applied followed by a decreasing ramp until reaching 15.8 $°C$ again, as illustrated in Fig. 6. As noted, the sample is initially in thermal equilibrium, where the heat flux is zero. This is followed by sensible heat flow when the PCM is still in its solid state. The curve then starts increasing gradually at a time corresponding to the onset of melting. The latent heat absorbed also increases gradually and the largest quantity is absorbed in the vicinity of the melting point. After complete melting, and reaching the constant heating phase, the PCM goes back to a thermal equilibrium, with no more flux variation, until the cooling ramp starts.

When cooling starts, the liquid PCM releases sensible heat until reaching the solidification temperature. The difference between the melting and solidification is that the majority of freezing happens directly, and the largest amount of latent heat is released at first, then the rest will solidify gradually. This behavior can be also regarded to the expected shape of the enthalpy curve. The portion around the curve at the solidification temperature is discontinuous. There is a direct energy jump from a temperature point in the liquid state to the solidification point. We note also the existence of supercooling, which is illustrated by the formation of a vertical portion or discontinuity in the curve (Fig. 1). After complete freezing, the PCM returns back to its equilibrium state with almost zero flux.

6. Results and discussion

As previously stated, the major aim is to first estimate the main thermo-physical properties and

485 to highlight their effect on the numerical results if the supercooling, convection, and soluble
486 impurities are ignored or not. To achieve this, we compare the numerical results, using an improved
487 model, with the experimental ones. The properties in Tables 1 and 2 and the verified thermo-
488 physical properties (conductivities, specific heat capacities, latent heat of fusion, thermal contact
489 resistance, etc.) are fixed in the model. It should be noted that the Boussinesq force has been varied
490 to account for convection, the melting temperature to calibrate the enthalpy curve, and the degree
491 of supercooling to estimate the nucleation temperature. In the following, some significant results
492 showing effects of physical phenomena are comprehensively presented and discussed.

493 **6.1. Effect of enthalpy curve shape**

494 As explained before, the presence of soluble impurities in the PCM results in a melting
495 temperature depression. Recall that, the used Octadecane is thought to be 99% pure. So, the 1% of
496 soluble impurities can have an impact on the heat flux curve. This will be investigated theoretically
497 and numerically. First, the depression in the melting temperature is calculated from Eq. (1) to obtain
498 T_m = 28.03 °C. Thus, the PCM melts with a depression of about 0.1 °C compared to the case of
499 pure Octadecane. Then, this melting temperature will be used in the numerical model, to check if
500 this the numerical and experimental fluxes match. If not, T_m will be changed until they well match.
501 The enthalpy-temperature curves are plotted in Fig. 7 for different values of (T_a - T_m). As
502 demonstrated, the curve becomes less steep as T_m deviates from T_a. This induces a melting
503 temperature range that causes a gradual increase in latent heat instead of absorbing it at once.
504 Moreover, to show the important impact of enthalpy curve on the flux, we compare the heat flux
505 obtained numerically for the case pure Octadecane to the experimental one (cf. Fig. 8a). In pure
506 PCM, there is no melting range. Thus, the immediate absorption of latent heat at the melting
507 temperature results in a sharp and high rate of heat flow at this moment, as shown in the comparison
508 curves. However, when there exists a temperature depression, the rate of heat absorption decreases
509 more, since there is no instant absorption and release. The accurate prediction of the onset of

melting and freeing is highly dependent on taking into account the real enthalpy-temperature relation.

By comparing the experimental and numerical curves, the best fit was obtained for T_m = 27.6 $°C$, which corresponds to a variation of about 0.5°C from the supposed pure melting temperature found in literature (Fig. 7). This shows that using Eq. (1) may not be adequate in our case but can be used as pre-estimation. Also, the supposed melting temperature [48, 49] of pure Octadecane is also questionable. If Octadecane is considered pure, the heat flux curve will show a high discrepancy when compared to the experimental one, as shown in Fig. 8a. The curve obtained numerically comes from considering the enthalpy curve as the traditional piece-wise function. This shows that such a curve cannot be used for our case.

The final numerical curve for melting is plotted in Fig. 11 despite the fact that this is the result from the enhanced numerical model, i.e. including also convection. In addition, we highlight that the heating rate does not influence the prediction of the melting point T_m, since the enthalpy curve is unique for a material.

6.2. Effect of presence of supercooling and convection

We show, in what follows, the discrepancy that would have resulted if we ignored the presence of convection and supercooling. The major effect of ignoring convection (cf. Fig. 9a) is on estimating the time of melting and mainly that of solidification. At first, the material is solid. So convection will start affecting the curve as soon as the liquid fraction starts increasing. It is important here to address the effectiveness of our partial bounce-back LBM model. By this method, we are able to treat the mushy zone as a porous medium, where the velocity of the fluid is restrained but not completely blocked. The Rayleigh number (Ra), corresponding to the real convection, is searched by a fitting method, and is found to be Ra = 1.2×10^4. Higher values would lead to an over estimation (Fig. 9b).

On the other hand, if supercooling is ignored (see Fig. 10a), the solidification starts before the real instant. So, the experimental and numerical results will show a lag in time. To overcome this,

536 we have sought the degree of supercooling through a tuning (fitting) method. Hereafter, the best
537 estimated degree of supercooling corresponds to 1.4 °*C*. If higher supercooling degree is used, the
538 supercooling phenomenon will be overestimated (see Fig. 10b).

539 By this, we can combine all the enhancements to the present model: using the real enthalpy
540 curve, including convection and supercooling, using variable thermo-physical properties for solid
541 and liquid phases, and using a partial bounce-back LBM for phase change to better simulate the
542 low effect of convection. The enhanced model calculated for $Ra = 1.2\times10^4$, degree of super cooling
543 of 1.4 °*C*, and a melting point depression of 0.43 °*C* is displayed in Fig. 11, and shows a great
544 improvement, and matches the experimental results.

545 The simplifications taken in some numerical models can result in an overall discrepancy in the
546 real behavior of PCM. These discrepancies may lead to wrong estimation of the fusion times and
547 the energy amount stored. Consequently, the PCM will not give the desired performance. The major
548 enhancement to the proposed model was to take into account natural convection, supercooling, to
549 adopt variable thermo-physical properties for solid and liquid phases, and to use the real enthalpy
550 curves corresponding to the considered PCM. These improvements have led to better agreement
551 with the experimental results, and showed that if the above phenomena were present, they cannot
552 be ignored.

553 **7. Conclusion**

554 The main aim of this work is to characterize the thermo-physical properties and performance of
555 Octadecane. This PCM may be promising for the usage in glass facades or other building materials
556 and latent heat systems. To achieve such an objective, we adopted an approach based on
557 experimental and numerical techniques. The enhanced numerical model, used here, can help
558 estimate some properties, and can be also used as an optimization tool for any practical application.

559 The thermo-physical properties obtained experimentally and, using the numerical model, match
560 the expected values from literature. The adopted numerical model is a thermal LBM with a partial

bounce-back approach and an enthalpy-based model. We considered the natural convection, supercooling, variable thermo-physical properties (when necessary), and the real enthalpy curve of Octadecane. Simulations performed using the improved model corroborate the experimental results and show that ignoring these phenomena may lead to wrong estimation of the fusion times and amount of energy stored and the PCM will not give the desired performance.

Disclosure statement

The authors declare no potential conflicts of interest regarding authorship and/or publication of this paper.

ORCIDs iD

Alissar Yehya https://orcid.org/0000-0001-9956-3636

Hassane Naji http://orcid.org/0000-0002-5994-7958

Laurent Zalewski https://orcid.org/0000-0002-7298-3224

References

[1] M. Hegger, M. Fuchs, T. Stark, and M. Zeumer, Energy Manual, Sustainable architecture. Edition Detail 2008, ISBN-10: 3764388307.

[2] Energy Efficiency Requirements in Building Codes, Energy Efficiency Policies for New Buildings, International Energy Agency, 2008.

[3] A. Castell, M. Medrano, J. Roca, A. Vila A, and L.F. Cabeza, Experimental Study of PCM in Mediterranean Buildings, Effstock 2009 Conference, Stockton University, 2009.

[4] A. Sharma, V.V. Tyagi, C.R. Chen, and D. Buddhi, Review on thermal energy storage with phase change materials and applications. Renew. Sust. Energy Rev., vol. 13, pp. 318-345, 2009.

[5] N. Soaresa, J. J. Costab, A. R. Gaspar, and P. Santos P, Review of passive PCM latent heat thermal energy storage systems towards buildings' energy efficiency, Energy Build., vol. 59, pp. 82-103, 2013.

586 [6] R. Baetens, B. P. Jelle, and A. Gustavsen, Phase change materials for building applications: a
587 state-of-the-art review, Energy Build., vol. 42, pp. 1361-1368, 2010.
588 [7] B. Zalba, J. M. Marín, L. F. Cabeza, and H. Mehling, Review on thermal energy storage with
589 phase change materials: Heat transfer analysis and applications, Appl. Therm. Eng., vol. 23,
590 pp. 51-83, 2003.
591 [8] M. M. Farid, A. M. Khudhair, S. A. K. Razack, and S. Al-Hallaj, A review on phase change
592 energy storage: materials and applications, Energy Convers. Manage., vol. 45, pp. 1597-1615,
593 2004.
594 [9] Y. Zhang, G. Zhou, K. Lin, Q. Zhang, and H. Di, Application of latent heat thermal energy
595 storage in buildings: State of the art and outlook, Build. and Environ., vol. 42, pp. 2197-2209,
596 2007.
597 [10] Y. Dutil, D. Rousse, N. Ben Salah, S. Lassue, and L. Zalewski, A review on phase-change
598 materials: Mathematical modeling and simulations, Renew. Sust. Energy Rev., vol. 15, pp.
599 112-130, 2011.
600 [11] V. R. Voller, C. R. Swaminathan, and B. G. Thomas, Fixed grid techniques for phase change
601 problems: a review. Int. J. Numer. Methods Eng., vol. 30, pp. 875-898, 1990.
602 [12] R.E. White, An enthalpy formulation of the Stefan problem, SIAM J. Numer. Analysis, vol.
603 19, pp. 1129-57, 1982.
604 [13] C. Bonacina, G. Comini, A. Fasano, and M. Primicerio, Numerical solution of phase-change
605 problems. Int. J. Heat Mass Transfer, vol. 16, pp. 1825-32, 1973.
606 [14] X. Zeng and A. Faghri, Temperature-transforming model for binary solid–liquid phase-
607 change problems, Part I: Mathematical modeling and numerical methodology, Numer. Heat
608 Transfer, Part B, vol. 25, pp. 467-80, 1994.
609 [15] F. Talati and M. Taghilou, Lattice Boltzmann application on the PCM solidification within a
610 rectangular finned container, Appl. Therm. Eng., vol. 83, pp. 108-120, 2015.

611 [16] M. Taghilou and F. Talati, Numerical investigation on the natural convection effects in the
612 melting process of PCM in a finned container using lattice Boltzmann, Int. J. Refrigeration,
613 vol. 70, pp. 157-170, 2016.
614 [17] A. R. Darzi, M. Jourabian, and M. Farhadi, Melting and solidification of PCM enhanced by
615 radial conductive fins and nanoparticles in cylindrical annulus, Energy Convers. Manage.,
616 vol.118, pp. 253-263, 2016.
617 [18] Y. Su and J. H. Davidson A new mesoscopic scale timestep adjustable non-dimensional
618 lattice Boltzmann method for melting and solidification heat, Int. J. Heat Mass Transfer, vol.
619 92, pp. 1106-1119, 2016.
620 [19] M. Jourabian and M. Farhadi, Melting of nanoparticles-enhanced phase change material
621 (NEPCM) in vertical semicircle enclosure: numerical study, J. Mech. Sci. Technology, vol.
622 29, no. 9, pp. 1-12, 2015.
623 [20] M. Jourabian, M. Farhadi, and K. Sedighi, On the expedited melting of phase change material
624 (PCM) through dispersion of nanoparticles in the thermal storage unit, Comput. Math. Appl.,
625 vol. 67, pp. 1358-1372, 2014.
626 [21] A. Yehya and H. Naji, Thermal lattice Boltzmann simulation of entropy generation within a
627 square enclosure for sensible and latent heat transfers, Appl. Sci., vol. 5, pp. 1904-1921,
628 2015.
629 [22] A. Yehya, H. Naji, L. Zalewski, Assessment of a Lattice Boltzmann Model to simulate fluid
630 flows with complex geometries, Computational Thermal Sciences, vol. 7 (2), 2015.
631 [23] A. Yehya and H. Naji, Towards the simulation of supercooling and convection in phase
632 change materials using a thermal lattice Boltzmann method, Prog. Comput. Fluid Dy., vol
633 18, 2018.
634 [23] Q. Li, K. H. Luo, Q. J. Kang, Y. L. He, Q. Chen, and Q. Liu, Lattice Boltzmann methods for
635 multiphase flow and phase-change heat transfer, Progress Energy Comb. Sci., vol. 52, pp.
636 62-105, 2016.

637 [24] V. R. Voller, Fast implicit finite-difference method for the analysis of phase change
638 problems, Numer. Heat Transfer, Part B, vol. 17, pp. 155-69, 1990.
639 [25] C. R. Swaminathan and V. R. Voller, Towards a general numerical scheme for solidification
640 systems, Int. J. Heat Mass Transfer, vol. 40, pp. 2859-68, 1997.
641 [26] D. Chatterjee, Lattice Boltzmann Modeling for Melting/Solidification Processes, In book:
642 Hydrodynamics - Optimizing Methods and Tools, Harry Schulz et al. (Eds.), ISBN: 978-953-
643 307-712-3, InTechopen, 2011. doi: 10.5772/28236
644 [27] S. N. AL-Saadi and Z. J. Zhai, Modeling phase change materials embedded in building
645 enclosure: A review. Renew. Sust. Energy Rev., vol. 21, pp. 659-673, 2013.
646 [28] M. Morgan, R. W. Lewis, and O. C. Zienkiewicz, An improved algorithm for heat conduction
647 problems with phase change, Int. J. Numer. Methods Eng., vol.12, pp. 1191-1195, 1978.
648 [29] C. Huber, A. Parmigiani, B. Chopard, M. Manga, and O. Bachmann, Lattice Boltzmann
649 model for melting with natural convection, Int. J. Heat Fluid Flow, vol. 29, pp. 1469-1480,
650 2008.
651 [30] M. Jourabian, M. Farhadi, and A. A. R. Darzi, Convection-dominated melting of phase
652 change material in partially heated cavity: lattice Boltzmann study, Heat Mass Transfer, vol.
653 49, pp. 555-565, 2013.
654 [31] A. Mezrhab, M. A. Moussaoui, M. Jami, H. Naji, and M. Bouzidi, Double MRT thermal lattice
655 Boltzmann method for simulating convective flows, Physics Letters A, vol. 374, pp. 3499-
656 3507, 2010.
657 [32] S. Chen and G.D. Doolen, Lattice Boltzmann Method for Fluid Flows, Annu. Rev. Fluid
658 Mech., vol. 30:329-364, 1998
659 [33] A. Xu, W. Shyy, T.S. Zhao, Lattice Boltzmann modeling of transport phenomena in fuel cells
660 and flow batteries, Acta Mech. Sin., vol. 33(3):555-574, 2017.
661 [34] A. Xu, L. Shi, T.S. Zhao, Accelerated lattice Boltzmann simulation using GPU and
662 OpenACC with data management, Int. J. Heat Mass Transfer, vol. 109, 577-588, 2017.

[35] D. Gao and Z. Chen, Lattice Boltzmann simulation of natural convection dominated melting in a rectangular cavity filled with porous media, Int. J. Therm. Sci., vol. 50, 493-501, 2011.

[36] D. Gao, Z. Chen, L. Chen, A thermal lattice Boltzmann model for natural convection in porous media under local thermal non-equilibrium conditions, Int. J. Heat Mass Transfer, vol. 70, 979-989, 2014.

[37] C. K. Schoff and R. L. Blaine, Purity determinations by thermal methods, STP 838, ASTM International (ed.), 1984.

[38] E. Franquet, S. Gibout, P. Tittelein, L. Zalewski, and J.-P. Dumas, Experimental and theoretical analysis of a cement mortar containing microencapsulated PCM, Appl. Therm. Eng., vol. 73, no. 1, pp. 32-40, 2014.

[39] S. Gibout, E. Franquet, J.-P. Bédécarrats, and J. -P. Dumas, Comparison of different modelings of pure substances during melting in a DSC experiment, Thermochim. Acta, vol. 528, pp. 1-8, 2012.

[40] J. -P. Dumas, S. Gibout, P. Cézac, E. Franquet, and D. Haillot, Model for the DSC thermograms of the melting of ideal binary solutions, Thermochim. Acta, vol. 57, pp. 64-76, 2013.

[41] S. Chapman and T. Cowling, The mathematical theory of non-uniform Gases, 3th ed., Cambridge University Press, Cambridge, 1970.

[42] Z. Guo, B. Shi, and C. Zheng, A coupled lattice BGK model for the Boussinesq equations, Int. J. Numer. Methods Fluids, vol. 39, no. 4, pp. 325-342, 2002.

[43] H. Chen and X. Shan, Simulation of nonideal gases and gas-liquid phase transitions by the lattice Boltzmann equation. Phys. Rev. E, vol. 49, pp. 2941-2948, 1994.

[44] L. -S. Luo, Lattice-Gas automata and lattice Boltzmann equations for two-Dimensional hydrodynamics, PhD Thesis, Georgia Institute of Technology, Atlanta, GA 30332, 1993.

687 [45] A. Yehya, H. Naji, and M. C. Sukop, Simulating flows in multi-layered and spatially-variable
688 permeability media via a new gray lattice Boltzmann model, Comp. Geotech., vol. 70, pp.
689 150-158, 2015.
690 [46] A. Yehya, Contribution to the experimental and numerical characterization of phase change
691 materials: Consideration of convection, supercooling, and soluble impurities, PhD Thesis
692 Univ. Artois/Applied Sciences' Faculty, F-62400 Béthune, France, 2015.
693 [47] T. Inamuro, M. Yoshino, H. Inoue, R. Mizuno, and F. A. Ogino, Lattice Boltzmann method
694 for a binary miscible fluid mixture and its application to a heat-transfer problem. J. Comput.
695 Phys., vol. 179, pp. 201-215, 2002.
696 [48] J. F. Messerly, G. B. Guthrie, S. S.Todd, and H. L. Finke, Low-temperature thermal data for
697 pentane, n-heptadecane, and n-octadecane. Revised thermodynamic functions for the n-
698 alkanes, C5-C18, J. Chem. Eng. Data, vol. 12, no., pp. 338-346, 1967.
699 [49] H. Mehling and L. F. Cabeza, Heat and cold storage with PCM: An up to date introduction
700 into basics and applications, Springer-Verlag, Berlin-Heidelberg, 2008.
701 [50] A. Joulin, L. Zalewski, S. Lassue, and H. Naji, Experimental investigation of thermal
702 characteristics of a mortar with or without a micro-encapsulated phase change material. Appl.
703 Therm. Eng., vol. 66, pp. 171-180, 2014.
704 [51] A. Joulin, Z. Younsi, L. Zalewski, S. Lassue, D. R. Rousse, and J. P Cavrot, Experimental
705 and numerical investigation of a phase change material: thermal-energy storage and release,
706 Appl. Energy, vol. 88, pp. 2454: 2462, 2011.
707 [52] M. Lachheb, Z. Younsi, H. Naji, M. Karkri, and S. Ben Nasrallah, Thermal behavior of a
708 hybrid PCM/plaster: A numerical and experimental investigation", Appl. Therm. Eng., vol.
709 111, pp. 49-59, 2017.

710 [53] L. Zalewski, S. Lassue, D. R. Rousse, A. Joulin, Z. Younsi, A novel technique for
711 experimental thermophysical characterization of phase-change materials, Int. J. Thermophys,
712 vol. 32, pp. 674-692, 2010.
713 [54] A. Tleoubaev A. and Brzezinski, Fast measurements of absolute thermal conductivity
714 excluding thermal contact resistance errors, LaserComp, Inc., 20 Spring Street, Saugus,
715 Massachusetts 01906, USA.
716 [55] A. Faghri, Y. Zhang, and J. R. Howell, Advanced Heat and Mass Transfer, Global Digital
717 Press, 2010.
718

List of Tables

Table 1. *Properties of Plexiglas* [48, 49]

Property	Value
Heat capacity	1470 $J.Kg^{-1}.K^{-1}$
Thermal conductivity	0.19 $W.(m.K)^{-1}$
Density	1190 $Kg.m^{-3}$

Table 2. *Properties of Octadecane from literature* [48, 49]

Property	Value
c_{solid}	1910 $JKg^{-1}°C^{-1}$
c_{liquid}	2230 $JKg^{-1}°C^{-1}$
Density ρ	779 Kgm^{-3}
λ_{solid}	0.356 $Wm°C^{-1}$
λ_{liquid}	0.149 $Wm°C^{-1}$
Enthalpy of fusion	241650 JKg^{-1}
Temperature of fusion	28.15 °C
β	0.02 K^{-1}
Pr	50

List of Figure Captions

Figure 1. Enthalpy-temperature relationship for pure PCMs with soluble impurities in the presence of supercooling.

Figure 2. Two-dimensional schematic of the studied sample.

Figure 3. (a) Schematic illustration of the experimental setup, (b) Schematic illustration of the studied sample.

Figure 4. Heat flux curves with no phase-change for (a) solid state, (b) liquid state.

Figure 5. Estimated thermal conductivity vs thermal contact resistivity: (a) solid state, (b) liquid state.

Figure 6. Heat flux curves indicating the presence of supercooling.

Figure 7. Enthalpy-temperature relationship for different (T_a - T_m) values.

Figure 8. (a) Effect of the presence of impurities on the heat flux, (b) Numerical and experimental shapes with T_m = 27.6 °C.

Figure 9. Effect of convection on the shape of the heat flux curve: (a) ignoring convection, (b) overestimating convection

Figure 10. Effect of supercooling on the shape of the heat flux curve: (a) ignoring supercooling, (b) overestimating supercooling

Figure 11. Experimental vs. numerical results when using the enhanced model.

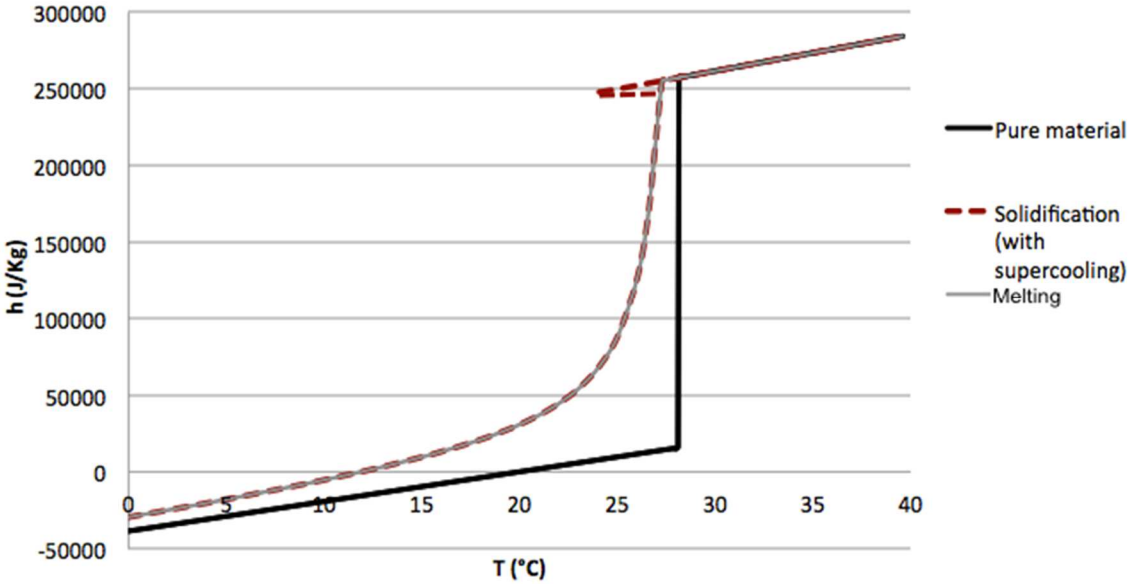

Figure 1. Enthalpy-temperature relationship for pure PCMs with soluble impurities in the presence of supercooling

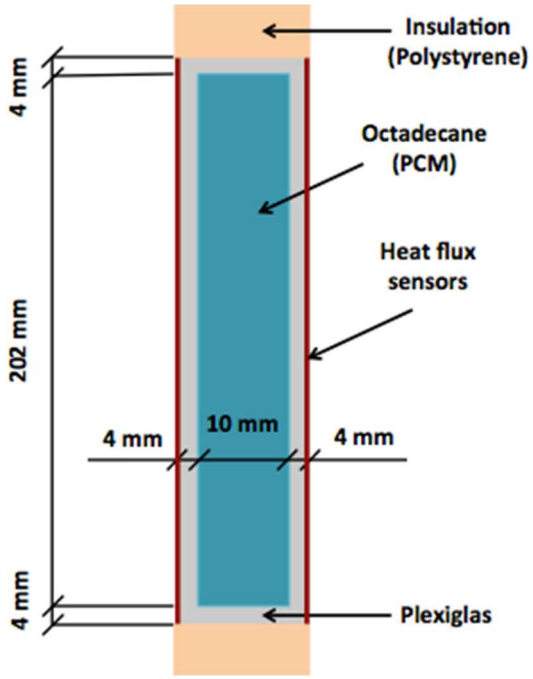

Figure 2. Two-dimensional schematic of the studied sample

759

760

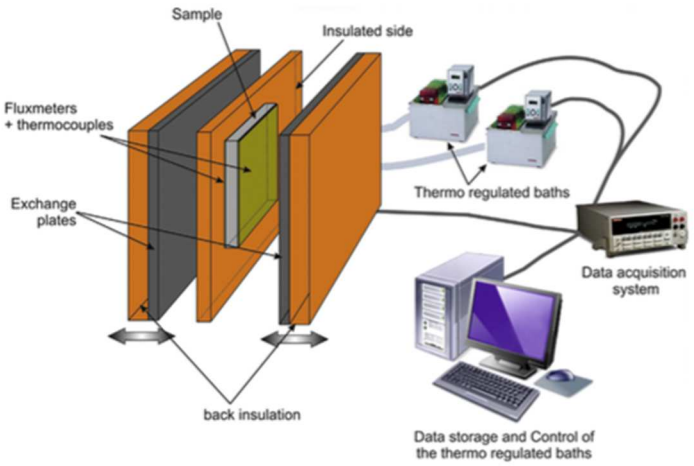

Figure 3a. Schematic illustration of the experimental setup

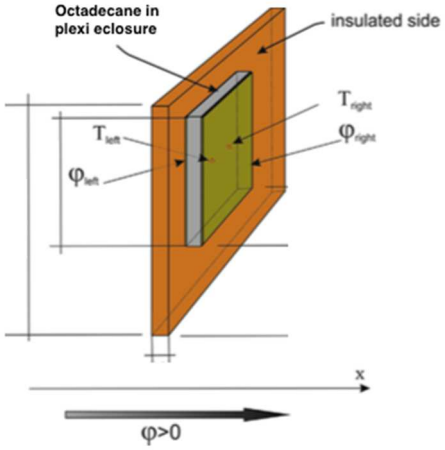

Figure 3b. Schematic illustration of the studied sample

761

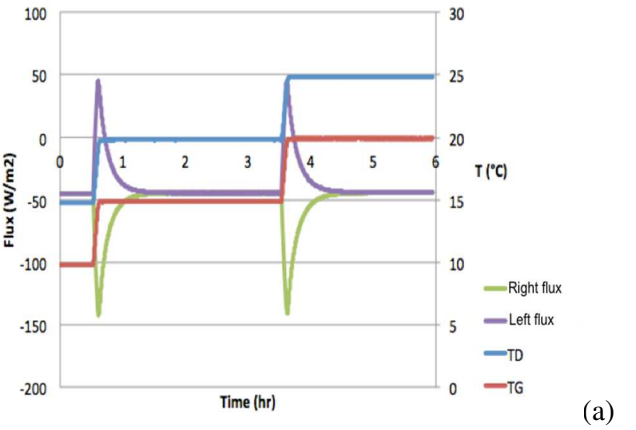

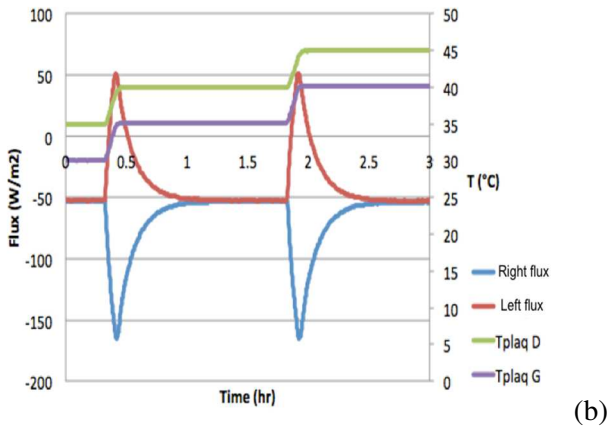

Figure 4. Heat flux curves with no phase-change for (**a**) solid state, (**b**) liquid state.

762

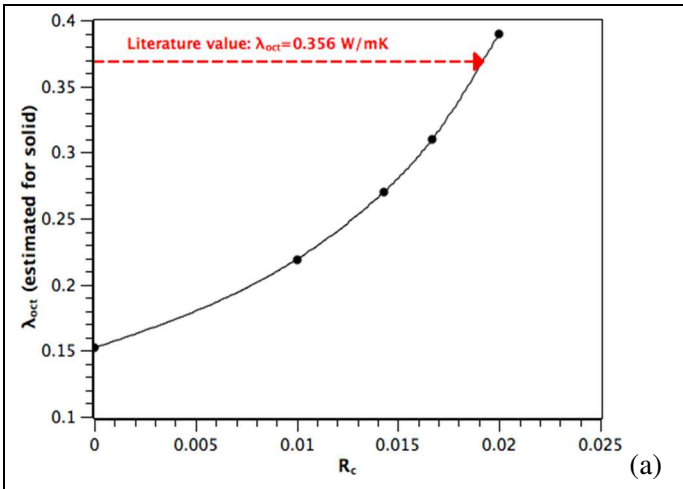

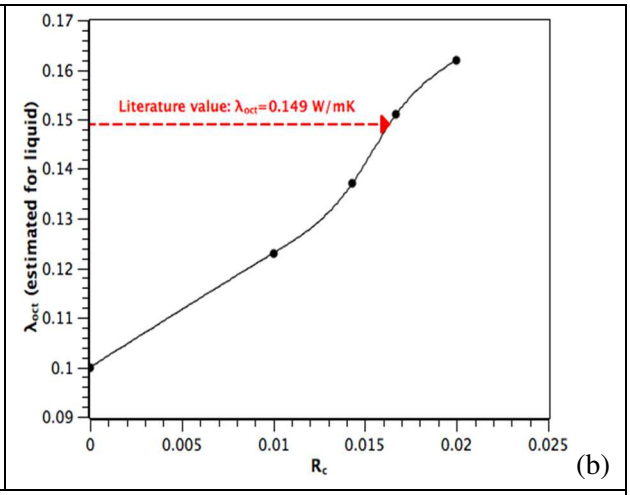

Figure 5. Estimated thermal conductivity vs. thermal contact resistivity: (a) solid state, (**b**) liquid state.

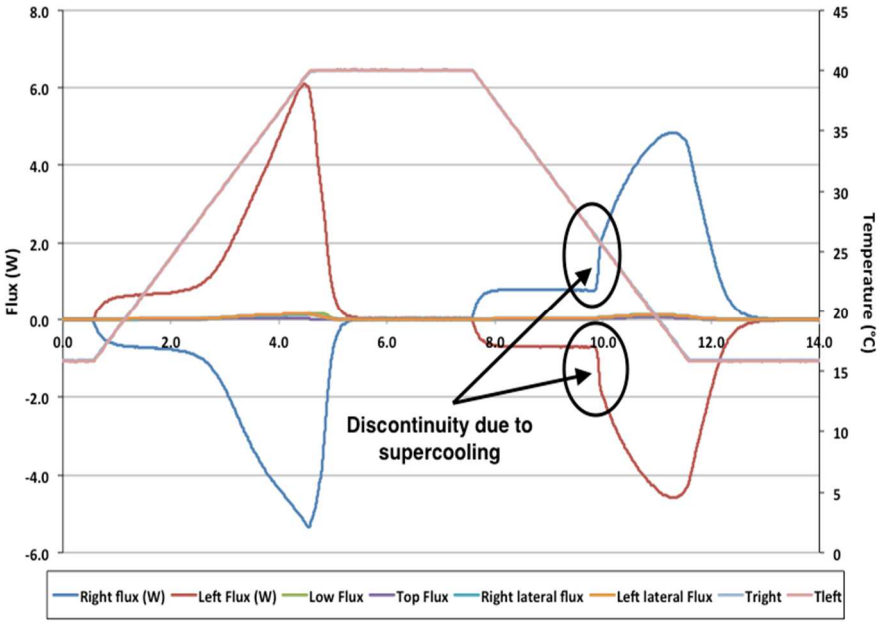

Figure 6. Heat flux curves indicating the presence of supercooling.

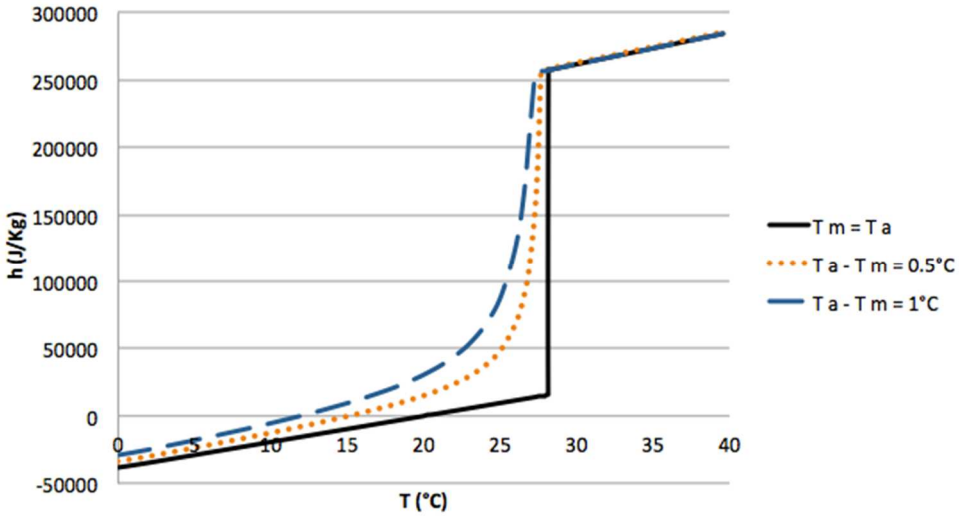

Figure 7. Enthalpy-temperature relationship for different (T_a - T_m) values.

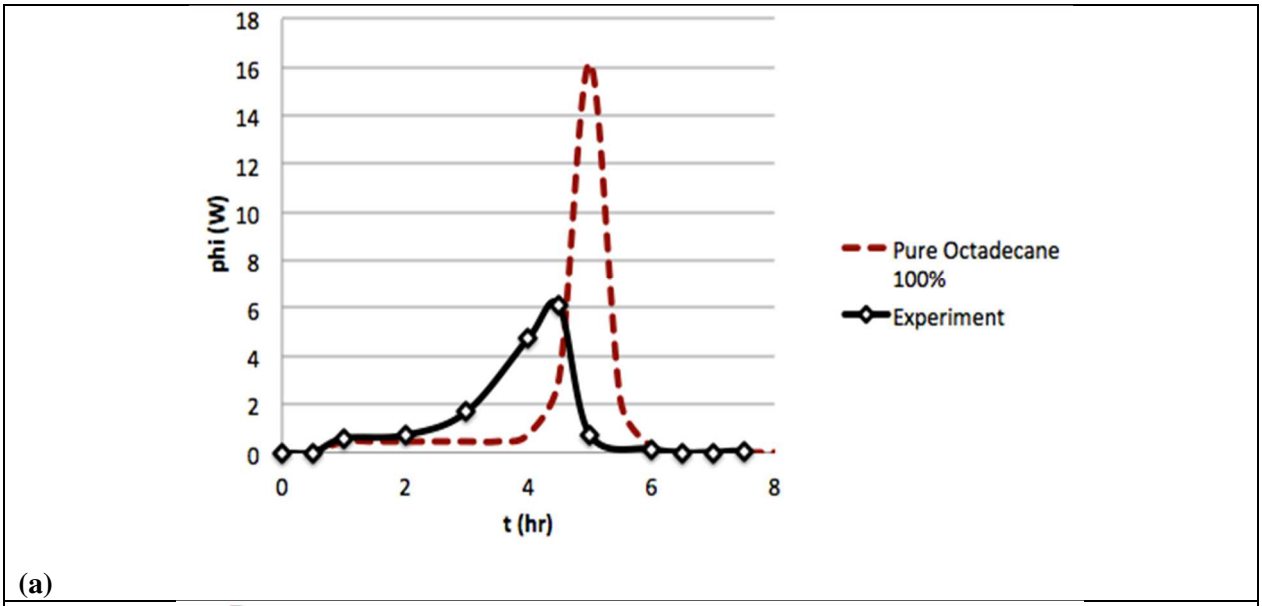

(a)

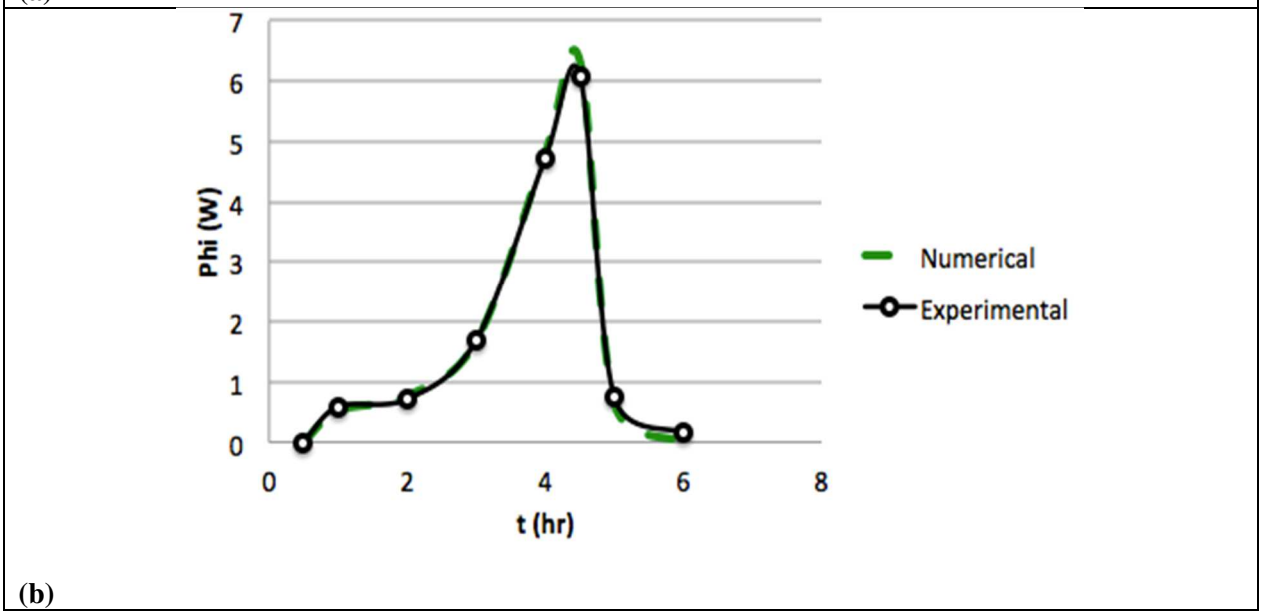

(b)

775

776 **Figure 8.** Effect of the presence of impurities on the heat flux (**a**), Numerical and experimental
777 shapes (**b**) with T_m = 27.6 °C
778
779

780

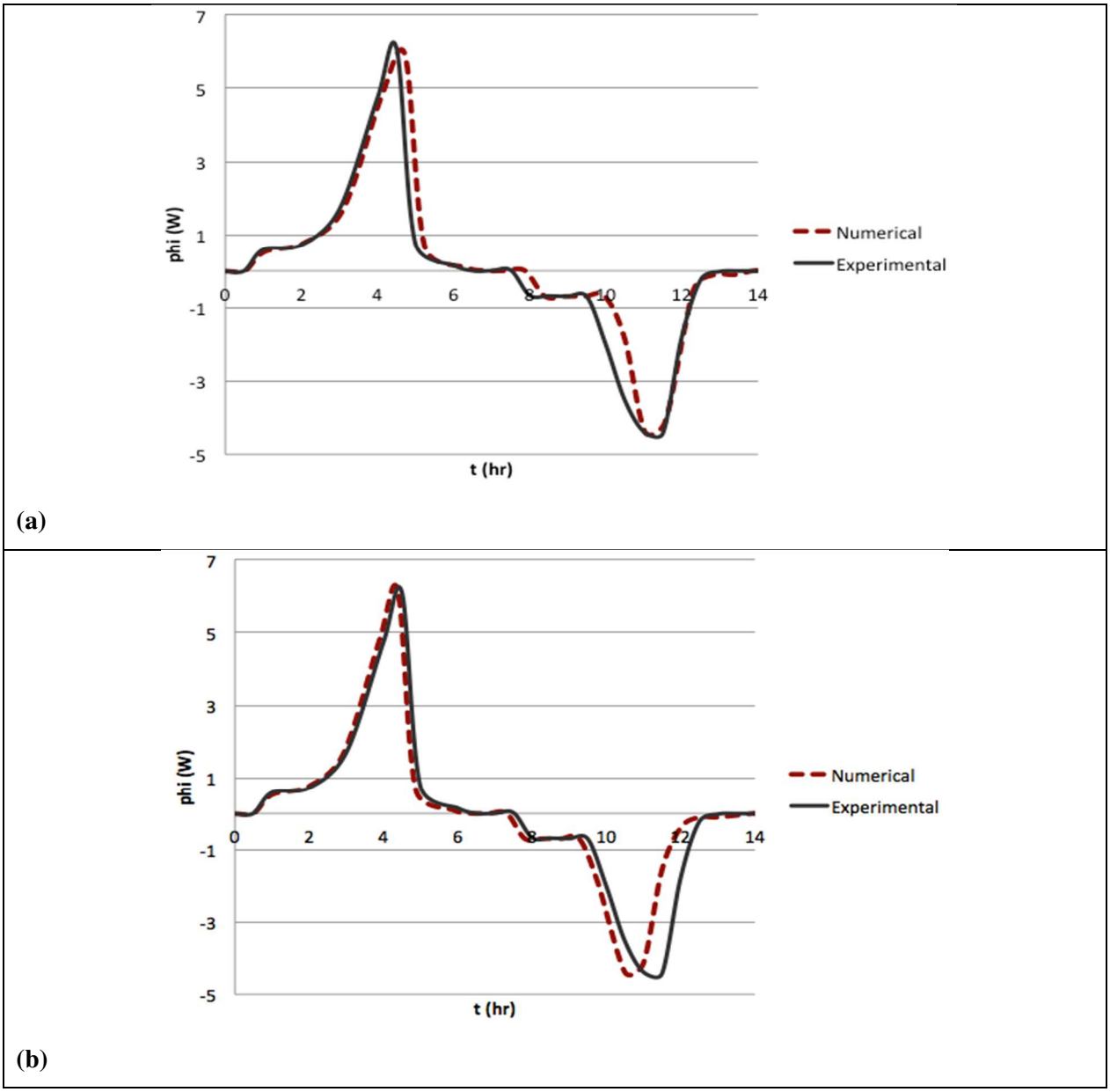

Figure 9. Effect convection on the shape of the heat flux curve: (**a**) ignoring convection, (**b**) overestimating convection

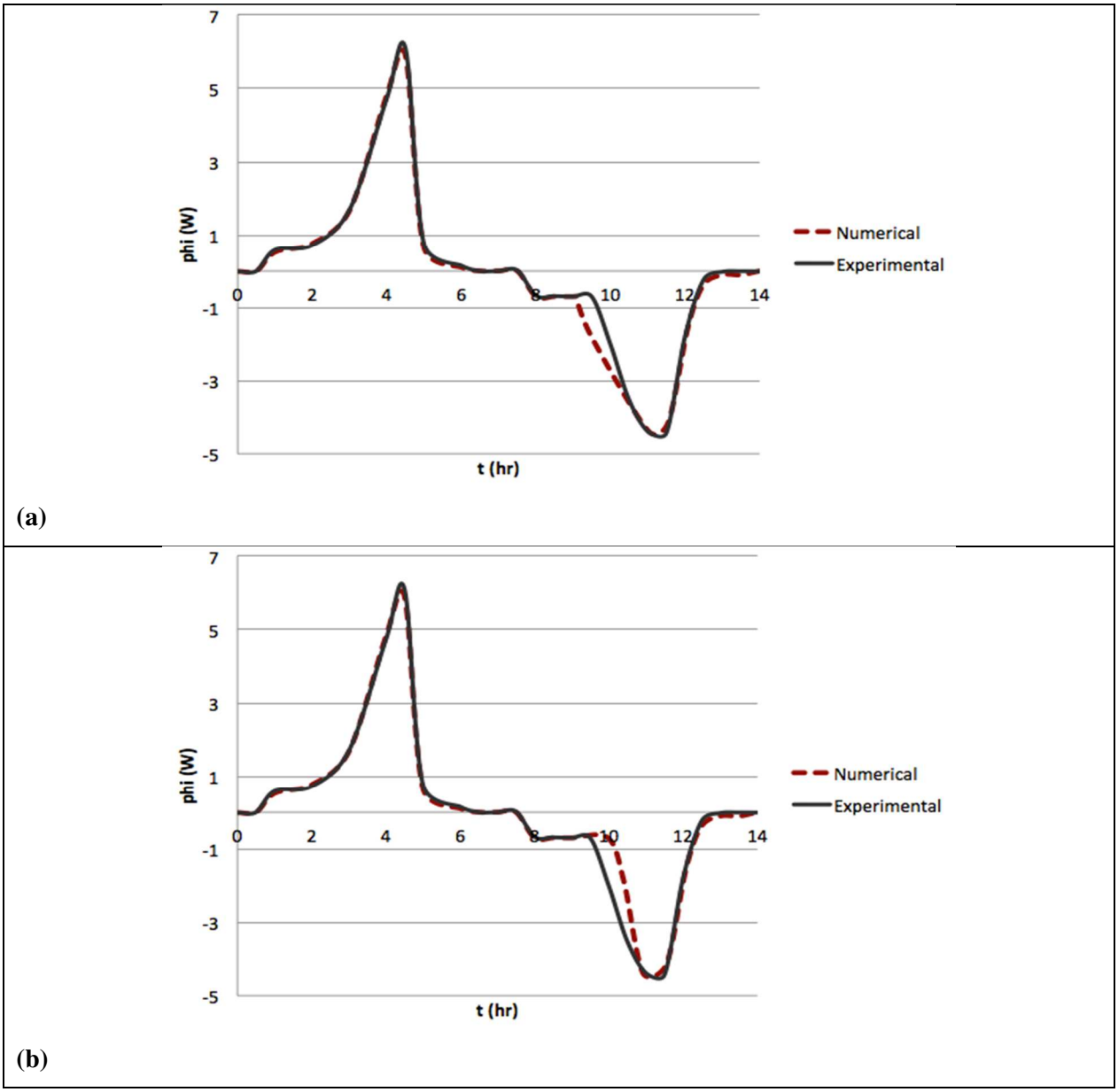

786
787
788 **Figure 10.** Effect supercooling on the shape of the heat flux curve: (**a**) ignoring supercooling, (**b**)
789 overestimating supercooling
790
791
792

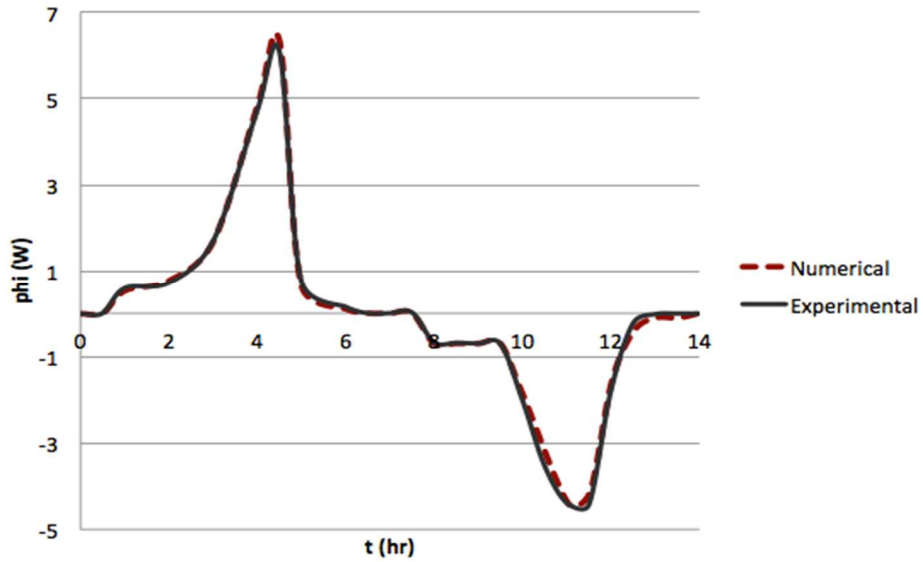

Figure 11. Experimental vs. numerical results when using the enhanced model.